9. Deformation Structures and Magnetic Fabrics at Site 1178: Implication for Deformation History Recorded in Accreted Sediments at an Evolved Portion of the Nankai Accretionary Prism[1]

Kohtaro Ujiie,[2] Toshio Hisamitsu,[3] Alex J. Maltman,[4]
Julia K. Morgan,[5] Mario Sánchez-Gómez,[6] and Harold J. Tobin[7]

[2]Institute for Frontier Research on Earth Evolution, Japan Marine Science and Technology Center, 3173-25 Showa-machi, Kanazawa-ku, Yokohama 236-0001, Japan. **ujiiek@jamstec.go.jp**
[3]Institute for Frontier Research on Earth Evolution, Japan Marine Science and Technology Center, 2-15 Natsushima-cho, Yokosuka 237-0061, Japan.
[4]Institute of Geography and Earth Sciences, University of Wales, Aberystwyth, Aberystwyth SY23 3DB, United Kingdom.
[5]Department of Geology and Geophysics, Rice University, MS-126, 6100 South Main Street, Houston TX 77005-1892, USA.
[6]Departamento de Geología, Universidad de Jaén, Virgen de la Cabeza 2, 23071 Jaén, Spain.
[7]Department of Earth and Environmental Science, New Mexico Institute of Mining and Technology, 801 Leroy Place, Socorro NM 87801, USA.

ABSTRACT

During Leg 190, accreted sediments at an evolved portion of the Nankai accretionary prism were penetrated. Deformation structures and anisotropy of magnetic susceptibility (AMS) data from Site 1178 indicate that structural and magnetic fabrics formed at the frontal part of the prism have been preserved, even ~65 km landward of the deformation front. As the sediments approached the deformation front, the bedding/fissility–parallel magnetic fabric took on a northeast-southwest–trending subhorizontal maximum AMS axis because of northwest-directed bedding-parallel compression. Subsequent faulting, represented by brecciated zones, took place at the frontal part of the accretionary prism, which is presumably equivalent to the imbricate thrusts in the prism. During this process, a steeply dipping bedding-oblique foliation developed in a fault zone, >100 m in thickness. The foliation was formed as a flattening plane associated with shearing deformation and alternates with brecciated zones, giving a geometric relationship similar to S-C or P-Y fabric. The magnetic fabric oriented parallel to the bedding-oblique foliation records pervasive strain related to faulting. Bedding and bedding-parallel magnetic fabric together with fissility were rotated about a horizontal axis during frontal accretion, re-

sulting in a seaward-verging magnetic fabric with northeast-southwest–trending subhorizontal maximum AMS axes. Overprinting of the deformation and/or modification of preexisting fabrics during subsequent rapid seaward growth of the Nankai accretionary prism has not been recorded in the accreted sediments at Site 1178, suggesting that later penetrative deformation was not significant at shallow burial depths in the prism.

INTRODUCTION

A number of Ocean Drilling Program (ODP) legs and associated geophysical surveys have investigated deformation, fluid flow, and physical properties in accretionary prisms. These studies have focused particularly on active processes at the toes of the prisms, improving our understanding of initial mountain building and related geophysical and geochemical processes (e.g., Moore and Vrolijk, 1992; Taira et al., 1992).

At the Nankai accretionary prism off Shikoku Island, southwest Japan, where a thick sequence of terrigenous sediment is being accreted, the prism and the incoming sedimentary section were penetrated at six sites during ODP Leg 190 (Moore, Taira, Klaus, et al., 2001; Moore et al., 2001) (Fig. F1A). One notable event during this leg was the penetration into an evolved portion of the prism at several upslope sites (Sites 1175, 1176, and 1178), located >40 km landward of the deformation front (Fig. F1). Although core recoveries of prism sediments at Sites 1175 and 1176 were very poor, Site 1178 achieved relatively high core recovery throughout. Site 1178 is located ~65 km landward of the deformation front and is halfway between the deformation front of the Nankai prism and the Shimanto accretionary complex on Shikoku Island, the ancient analog of the Nankai accretionary prism (Taira et al., 1988). Thus, cores from Site 1178 provide a rare opportunity to examine not only the structural evolution of the Nankai prism but also some of the geological characteristics of the "proto-Shimanto" complex. Moreover, Site 1178 recorded the deformation of shallowly buried (<1 km) but relatively evolved sediments in the accretionary prism, which are rarely preserved in onland accretionary complexes because of later overprinting and denudation. Therefore, we carried out detailed structural and magnetic fabric analyses on samples and data collected from Site 1178.

GEOLOGICAL CONTEXT OF SITE 1178

Site 1178 is located within the landward-dipping reflector zone (LDRZ) of the Nankai prism, characterized by landward-dipping, semicontinuous reflectors on seismic profiles (Fig. F1B). Site 1178 penetrated both slope and accreted sediments. Slope sediments extend from the seafloor to 200 meters below the seafloor (mbsf) and are composed mainly of hemipelagic mud, sandy mud, volcanic ash, and slump layers. Accreted sediments extend from ~200 mbsf to the bottom of Site 1178 (673 mbsf) and are composed mainly of sandy and muddy turbidites, interpreted as axial trench- and outer trench–wedge facies, respectively. Based on calcareous nannofossil biostratigraphy, the slope sediments range in age from Pleistocene to Pliocene, whereas the accreted sediments are late Miocene in age (Moore, Taira, Klaus, et al., 2001). Our study focused on the accreted sediments below 200 mbsf.

K. Ujiie et al.
Deformation Structures and Magnetic Fabrics

3
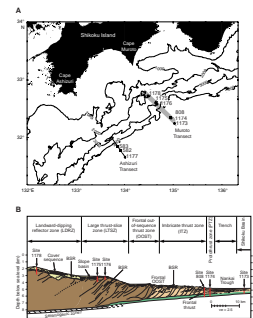
METHODS

Core-scale deformational features were described on board ship. The materials used for postcruise study were commonly fragile. Thus, the samples for optical microscopic examination were impregnated with a low-viscosity epoxy resin and dried in an oven. Thin sections were then made using standard methods. Samples for scanning electron microscope (SEM) examination were dipped into ethanol, then *t*-butyl alcohol, freeze-dried with liquid nitrogen, and dried in a vacuum evaporator. This drying method has been recommended for poorly consolidated clayey samples (Takizawa et al., 1995). After drying, samples were fractured to expose fresh surfaces and mounted on metallic stubs with liquid graphite. They were then coated with gold for secondary mode SEM examination.

Two oriented discrete samples were routinely collected from each section of the working half of the core for magnetic fabric analysis. Using these samples, the anisotropy of magnetic susceptibility was measured with a KLY-3 Kappabridge magnetic susceptibility meter, which was installed at Japan Marine Science and Technology Center.

DEFORMATION STRUCTURES IN ACCRETED SEDIMENTS

Brecciated Zone and Associated Structures

Figure F2 shows the variation of dip angles of Site 1178 deformation structures with depth. In accretionary prisms, gentle to moderate bedding dips are common. Increased deformation is recorded between 400 and 506 mbsf and from 622 to 673 mbsf (base of Site 1178). These two deformed intervals are marked by fractures and brecciated zones, in which the sediments are broken into millimeter- to centimeter-scale polished and slickenlined fragments (Fig. F3A). The brecciated zones are <10 m in thickness, and their intensity varies within the deformed intervals. Zones of black seams or weblike structures are locally observed near the brecciated zones. Under the optical microscope, the black seams are characterized by a marked preferred orientation of phyllosilicates parallel to the seam boundaries (Fig. F3B, F3C). The seams are planar, straight, and subparallel to each other and show spaced foliation-like features (Labaume et al., 1997) (Fig. F3B). However, locally they form networks, bifurcating, and oriented in two directions. Some of the seams show signs of shearing, with en echelon geometry or displaced sandy portions (Fig. F3C). Toward the base of the deformed interval at 506 mbsf, the spacing between fractures tends to decrease to a millimeter scale and downdip slickenlines become common. Locally, the closely spaced fractures display anastomosing or complex network forms, giving the appearance of a scaly fabric. The density of the fractures and the bedding dips rapidly decreases below 506 mbsf (Fig. F2). An increase in fracturing and brecciation is also seen at 550 mbsf.

Foliations

Foliations are mostly developed below 400 mbsf (Fig. F2). On a microscopic scale, the foliations are defined by the alignment of phyllosil-

F2. Bedding, foliation, and fractures, p. 12.
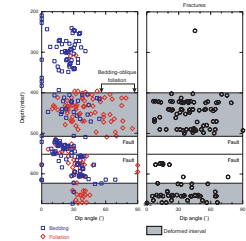
F3. Deformation structures, p. 13.
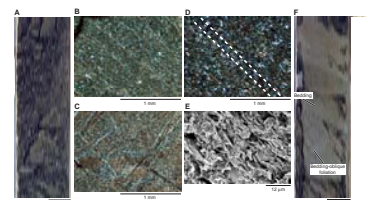
icates and clastic grains (Fig. F3D, F3E). Many of the foliations are considered to be fissility because they are parallel to the bedding (Fig. F3D) and are present in the undeformed intervals. However, a steeply dipping (>55°) bedding-oblique foliation is also developed, mostly in the deformed interval between 400 and 506 mbsf (Figs. F2, F3E, F3F). It does not appear to be an axial-planar cleavage because there is no evidence of folding. It is observed in intervals that alternate with brecciated zones. No asymmetric fabrics or shear bands are associated with the bedding-oblique foliation (Fig. F3F). The sets of polished and lineated shear surfaces in the brecciated zones, which are marked by the preferred orientation of minerals, crosscut the bedding-parallel fissility and/or bedding-oblique foliation, indicating that the brecciation was superposed on the planar fabrics.

MAGNETIC FABRICS IN ACCRETED SEDIMENTS

We measured the anisotropy of magnetic susceptibility (AMS) to determine the magnetic fabric in this evolved portion of the prism. The AMS is expressed by a symmetrical second-order tensor and is geometrically represented as an ellipsoid that is commonly coaxial with the strain ellipsoid (e.g., Borradaile, 1988). The AMS ellipsoid has three principal susceptibility axes: maximum susceptibility (K_{max}), intermediate susceptibility (K_{int}), and minimum susceptibility (K_{min}). The plane normal to K_{min} commonly expresses the magnetic foliation. The AMS ellipsoid reflects a statistical alignment of magnetic minerals, and the most magnetically susceptible minerals can have distributions of shape orientation or lattice orientations influenced by the kinematic history of the fabric, which leads to a relationship between AMS and structural fabrics. However, AMS can also be influenced by the magnetic mineral composition of rocks or sediments rather than by their fabric or strain (Borradaile, 1988).

Detailed rock magnetic tests identified that the carrier of AMS at Site 1178 is greigite (Hisamitsu et al., unpubl. data). Although the AMS of greigite-bearing sediments remains poorly understood, the AMS data of the accreted sediments at Site 1178 show a good correlation with the structural data (Fig. F4A). The magnetic foliation is parallel to bedding and bedding-parallel foliation (fissility), showing variable dips with depth. A distinct magnetic foliation is well correlated with the steeply dipping bedding-oblique foliation in the deformed interval between 400 and 506 mbsf. Magnetic foliation dips decrease rapidly across the base of the deformed interval at 506 mbsf. In contrast to the magnetic foliation, magnetic susceptibility is fairly uniform throughout the accreted sediments at Site 1178 (Fig. F4A). This strongly suggests that the changes in magnetic fabric with depth do not reflect mineralogical changes but instead represent the development of structures in the accreted sediments.

Based on the paleomagnetic directions of the samples, the orientation of AMS axes can be restored to their original positions before drilling. Despite the variable magnetic foliation dips, the corrected K_{max} axes are subhorizontal and dominantly oriented northeast-southwest, whereas the corrected K_{int} axes are shallowly to steeply inclined and oriented perpendicular to the K_{max} axes directions (Fig. F4B). The corrected K_{min} axes are shallowly to steeply inclined and dominantly oriented

F4. Magnetic susceptibility, dip angle, bedding, and foliation vs. depth, p. 14.
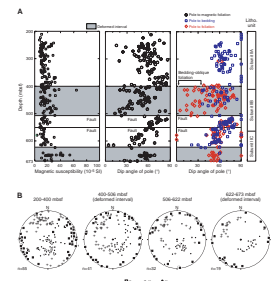
southeastward, which is consistent with the distribution of the poles to bedding and the foliation below 400 mbsf (Moore, Taira, Klaus, et al., 2001).

ORIGIN OF DEFORMATION STRUCTURES AND MAGNETIC FABRICS

Many of the magnetic foliations in the prism are parallel to bedding/fissility (Fig. F4A). Magnetic foliations dip variably, but the K_{max} axes are subhorizontal and mainly oriented northeast-southwest (Fig. F4B). These features indicate that the bedding-parallel magnetic fabrics with the subhorizontal northeast-southwest–trending K_{max} axes and the fissility were rotated about a horizontal axis. The orientations of the K_{max} axes might record the paleocurrent direction along the Nankai Trough. However, this possibility is unlikely because we took the AMS samples from clay/clayey silt, which does not normally record a current-induced depositional fabric. Alternatively, the bedding-parallel magnetic fabrics with northeast-southwest–trending subhorizontal K_{max} axes could reflect the modification of an initial bedding/compaction grain fabric by bedding-parallel (horizontal) compression near the deformation front (Graham, 1966; Owens, 1993). In this case, the subhorizontal K_{max} axes move within the bedding plane into the intermediate-strain direction, which is perpendicular to the plate-convergence direction. Such tectonic mineral fabric is expected to develop prior to rotation of bedding/fissility caused by frontal accretion. In addition, greigite was identified as a dominant magnetic mineral in the sediments prior to frontal accretion (Site 1177) and in the accreted trench-wedge facies near the deformation front (Site 1174) (Moore, Taira, Klaus, et al., 2001; Hisamitsu et al., unpubl. data). Therefore, we consider that the bedding-parallel magnetic fabric was formed during bedding-parallel (horizontal) compression near the deformation front and rotated about a horizontal axis during frontal accretion, resulting in a seaward-verging magnetic fabric with a northeast-southwest–trending subhorizontal K_{max} axis. Following this interpretation, the plate convergence vector at the time of frontal accretion can be inferred from the distribution of the principal susceptibility axes (Fig. F4B). The inferred plate convergence vector trends northwest, consistent with the present plate-convergence vector (Seno, 1977).

The intensity of fractures and brecciated zones in the deformed intervals and at 550 mbsf suggest that they represent faults in the accretionary prism. Based on calcareous nannofossil biostratigraphy, inversions of biostratigraphic age are apparent in the accretionary prism (Moore, Taira, Klaus, et al., 2001). Therefore, some of the brecciated zones in the deformed intervals are likely to be imbricate thrusts in the prism. The microscopic appearance of black seams displaying signs of shear and spaced foliationlike features (Fig. F3B, F3C) and their distribution near brecciated zones suggests that the zones of black seams are incipient breccia. Intense brecciation above 506 mbsf, together with a decrease in fracture density and in bedding and magnetic foliation dips below 506 mbsf (Figs. F2, F4A), imply that there is a major fault at the base of the deformed interval between 400 and 506 mbsf. However, there is no significant change in biostratigraphic age across the inferred major fault at 506 mbsf (Moore, Taira, Klaus, et al., 2001).

In the deformed interval between 400 and 506 mbsf, the bedding-oblique foliation alternates with brecciated zones. A plausible origin for the bedding-oblique foliation is the flattening associated with shearing in a fault zone >100 m in thickness. In this case, the magnetic fabric parallel to bedding-oblique foliation represents pervasive strain in the fault zone above 506 mbsf. Considering that the maximum principal compressive stress in an accretionary prism is commonly subhorizontal (Davis et al., 1983) and that the K_{max} axes are subhorizontal (Fig. F4B), a steeply dipping bedding-oblique foliation may develop perpendicular to the principal shortening direction. Thus, the geometric relationship between the bedding-oblique foliation and the brecciated zones appears to be analogous to the relationship between S- and C-surfaces in S-C mylonite (Berthé et al., 1979; Lister and Snoke, 1984) or P- and Y-surfaces in fault gouge (Rutter et al., 1986). No dissolution residues or pressure shadows associated with clastic grains are seen in the deformed interval between 400 and 506 mbsf (Fig. F3E), suggesting that pressure solution was not operative during the development of the bedding-oblique foliation. The bedding-oblique foliation is present in shallowly buried and poorly lithified sediments with porosities ranging from 30% to 40% (Moore, Taira, Klaus, et al., 2001). Presumably, reoriented detrital and/or diagenetic phyllosilicates define the bedding-oblique foliation. The fault at 550 mbsf and the brecciated zones in the deformed interval between 622 and 673 mbsf are not accompanied by a fault-related planar fabric, indicating the localized nature of deformation within the prism.

A summary of the overall distribution of deformation structures and magnetic fabrics with depth is shown in Figure F5. The bedding-parallel magnetic fabric formed by northwest-directed horizontal compression at the prism toe is developed throughout the accretionary prism section. Most of the brecciated zones are distributed in two deformed intervals, one of which (400–506 mbsf) preserves a fault-related planar fabric (bedding-oblique foliation) and a magnetic fabric oriented parallel to the bedding-oblique foliation, reflecting pervasive strain related to faulting in the accretionary prism.

TIMING OF DEFORMATIONS RECORDED IN ACCRETED SEDIMENTS AT AN EVOLVED PORTION OF THE NANKAI ACCRETIONARY PRISM

Despite the deformation within the accretionary prism, porosity at Site 1178 decreases gradually from ~63%–70% at the seafloor to 26%–35% at 673 mbsf, a typical burial-compaction trend across slope and accreted sediments (Moore, Taira, Klaus, et al., 2001). At the toe of the Nankai accretionary prism (Site 808) (Fig. F1), however, the offset along the active frontal thrust has disturbed the preexisting porosity profile (Shipboard Scientific Party, 1991). A disturbed preexisting porosity profile is not present at Site 1178. This requires that stress has been applied long enough for fluid to seep away and that recently active faulting did not occur at Site 1178. In contrast to the large thrust-slice zone (LTSZ), where active out-of-sequence thrusts develop, no faults appear to cross-cut slope sediments imaged in a seismic profile across the LDRZ (Fig. F1B). This suggests that faulting at Site 1178 occurred before deposition of the slope sediments prior to 5.54 Ma. One of the main results of drill-

F5. Deformation structures and magnetic fabric, p. 15.
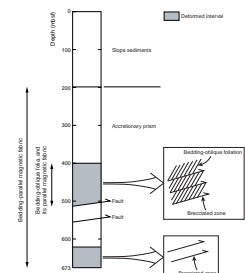
ing during ODP Leg 190 is the recognition of the rapid seaward growth of the Nankai accretionary prism; the outer 40 km of the prism (from the LTSZ to the prism toe) accreted within the past 2 m.y. (Moore, Taira, Klaus, et al., 2001). Therefore, faulting at Site 1178 is considered to have occurred when Site 1178 was located at the frontal part of the accretionary prism. The repetitions in biostratigraphy suggest that the faults at Site 1178 formed in association with the development of in-sequence thrusts at the frontal part of the prism. At Sites 1174 and 808 (Fig. F1), deformation bands appear to reflect pervasive strain related to faulting at the toe of the Nankai accretionary prism (Taira et al., 1992; Moore, Taira, Klaus, et al., 2001; Ujiie et al., in press). Although the deformation style is different, the bedding-oblique foliation in the deformed interval (400–506 mbsf) may record pervasive strain associated with faulting at the frontal part of the prism.

The timing of faulting and magnetic fabric development at Site 1178 implies that tectonic fabrics formed at the frontal part of the Nankai accretionary prism have been preserved ~65 km landward of the deformation front. Studies of ancient accretionary complexes have shown that offscraped sequences buried more than a few kilometers document the progressive development of tectonic fabrics during frontal accretion and the subsequent penetrative deformations associated with intraprism compression (e.g., in the Tertiary Shimanto accretionary complex) (DiTullio and Byrne, 1990; Ujiie, 1997; Lewis and Byrne, 2001). By contrast, the accreted sediments at Site 1178 do not record any modification of preexisting tectonic fabrics and/or overprinting of deformation during subsequent rapid seaward growth of the Nankai accretionary prism. This suggests that penetrative deformation associated with seaward growth of the prism was not significant at shallow burial depths in the prism.

CONCLUSIONS

At shallow burial depths, accreted sediments at an evolved portion of the accretionary prism do not present a formidably complicated structural pattern with polyphase overprinting deformation events but, instead, preserve early deformation structures and magnetic fabrics that formed at the frontal part of the prism. Magnetic fabric formed near the deformation front was simply rotated about a horizontal axis during frontal accretion. A bedding-oblique foliation in poorly lithified and shallowly buried sediments most likely consists of reoriented detrital and/or diagenetic phyllosilicates. This foliation appears to have developed as a flattening plane associated with shearing deformation and alternates with brecciated zones in a fault zone >100 m thick, displaying the geometric relationship of S-C or P-Y fabrics. The formation of a bedding-oblique foliation is considered to reflect initial strain localization related to faulting at the frontal part of the prism.

ACKNOWLEDGMENTS

REFERENCES

Berthé, D., Choukrome, P., and Jegouzo, P., 1979. Orthogneiss, mylonite and non-coaxial deformation and granites: the examples of South American shear zone. *J. Struct. Geol.,* 1:31–42.

Borradaile, G.J., 1988. Magnetic susceptibility, petrofabrics and strain. *Tectonophysics,* 156:1–20.

Davis, D., Suppe, J., and Dahlen, F.A., 1983. Mechanics of fold-and-thrust belts and accretionary wedges. *J. Geophys. Res.,* 88:1153–1172.

DiTullio, L., and Byrne, T., 1990. Deformation paths in the shallow levels of an accretionary prism: the Eocene Shimanto belt of southwest Japan. *Geol. Soc. Am. Bull.,* 102:1420–1438.

Graham, J.W., 1966. Significance of magnetic anisotropy in Appalachian sedimentary rocks. *In* Steinhard, J.S., and Smith, T.J. (Eds.), *The Earth Beneath the Continents.* Geophys. Monogr., Am. Geophys. Union, 10:627–648.

Labaume, P., Maltman, A.J., Bolton, A., Tessier, D., Ogawa, Y., and Takizawa, S., 1997. Scaly fabrics in sheared clays from the décollement zone of the Barbados accretionary prism. *In* Shipley, T.H., Ogawa, Y., Blum, P., and Bahr, J.M. (Eds.), *Proc. ODP, Sci. Results,* 156: College Station, TX (Ocean Drilling Program), 59–77.

Lewis, J.C., and Byrne, T., 2001. Fault kinematics and past plate motions at a convergent plate boundary: Tertiary Shimanto Belt, southwest Japan. *Tectonics,* 20:548–65.

Lister, G.S., and Snoke, A.W., 1984. S-C mylonites. *J. Struct. Geol.,* 6:617–638.

Moore, G.F., Taira, A., Klaus, A., et al., 2001. *Proc. ODP, Init. Repts.,* 190 [CD-ROM]. Available from: Ocean Drilling Program, Texas A&M University, College Station TX 77845-9547, USA.

Moore, G.F., Taira, A., Klaus, A., Becker, L., Boeckel, B., Cragg, B.A., Dean, A., Fergusson, C.L., Henry, P., Hirano, S., Hisamitsu, T., Hunze, S., Kastner, M., Maltman, A.J., Morgan, J.K., Murakami, Y., Saffer, D.M., Sánchez-Gómez, M., Screaton, E.J., Smith, D.C., Spivack, A.J., Steurer, J., Tobin, H.J., Ujiie, K., Underwood, M.B., and Wilson, M., 2001. New insights into deformation and fluid flow processes in the Nankai Trough accretionary prism: results of Ocean Drilling Program Leg 190. *Geochem. Geophys. Geosyst.,* 2:10.129/2001GC000166.

Moore, J.C., and Vrolijk, P., 1992. Fluids in accretionary prisms. *Rev. Geophys.,* 30:113–135.

Owens, W.H., 1993. Magnetic fabric studies of samples from Hole 808C, Nankai Trough. *In* Hill, I.A., Taira, A., Firth, J.V., et al., *Proc. ODP, Sci. Results,* 131: College Station, TX (Ocean Drilling Program), 301–310.

Rutter, E.H., Maddock, R.H., Hall, S.H., and White, S.H., 1986. Comparative microstructures of natural and experimentally produced clay-bearing fault gouges. *Pure Appl. Geophys.,* 124:3–30.

Seno, T., 1977. The instantaneous rotation vector of the Philippine Sea plate relative to the Eurasian plate. *Tectonophysics,* 42:209–226.

Shipboard Scientific Party, 1991. Site 808. *In* Taira, A., Hill, I., Firth, J.V., et al., *Proc. ODP, Init. Repts.,* 131: College Station, TX (Ocean Drilling Program), 71–269.

Taira, A., Katto, J., Tashiro, M., Okamura, M., and Kodama, K., 1988. The Shimanto Belt in Shikoku, Japan: evolution of Cretaceous to Miocene accretionary prism. *Mod. Geol.,* 12:5–46.

Taira, A., Hill, I., Firth, J., Berner, U., Brückmann, W., Byrne, T., Chabernaud, T., Fisher, A., Foucher, J.-P., Gamo, T., Gieskes, J., Hyndman, R., Karig, D., Kastner, M., Kato, Y., Lallement, S., Lu, R., Maltman, A., Moore, G., Moran, K., Olaffson, G., Owens, W., Pickering, K., Siena, F., Taylor, E., Underwood, M., Wilkinson, C., Yamano, M., and Zhang, J., 1992. Sediment deformation and hydrogeology of the Nankai accretionary prism: synthesis of shipboard results of ODP Leg 131. *Earth Planet. Sci. Lett.,* 109:431–450.

Takizawa, S., Kawata, T., and Ohono, Y., 1995. A method of fixation and freeze drying of soft sediments containing water. *Chishitsugaku Zasshi,* 101:941–944.

Ujiie, K., 1997. Off-scraping accretionary process under the subduction of young oceanic crust: the Shimanto Belt of Okinawa Island, Ryukyu arc. *Tectonics,* 16:305–322.

Ujiie, K., Maltman, A.J., and Sánchez-Gómez, M. in press. Origin of deformation bands in argillaceous sediments at the toe of the Nankai accretionary prism, southwest Japan. *J. Struct. Geol.*

Figure F1. A. Location map showing Leg 190 (solid circles) drilling sites, previous drilling sites (solid squares), and a three-dimensional seismic survey (shaded outline) off Shikoku Island, southwest Japan. **B.** Generalized depth section from seismic reflection data in the Muroto Transect showing tectonic domains and the location of Legs 131 and 190 drilling sites (after Moore, Taira, Klaus, et al., 2001). BSR = bottom-simulating reflector, ve = vertical exaggeration.

A
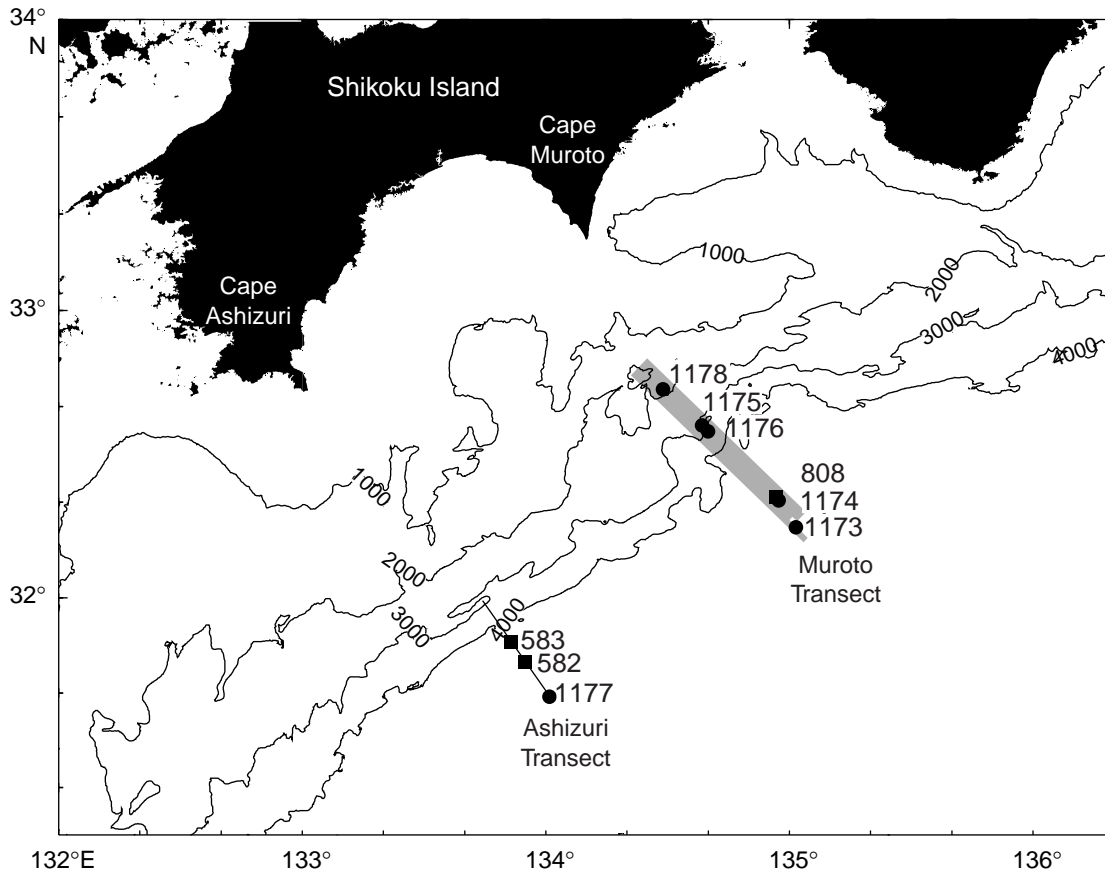
B
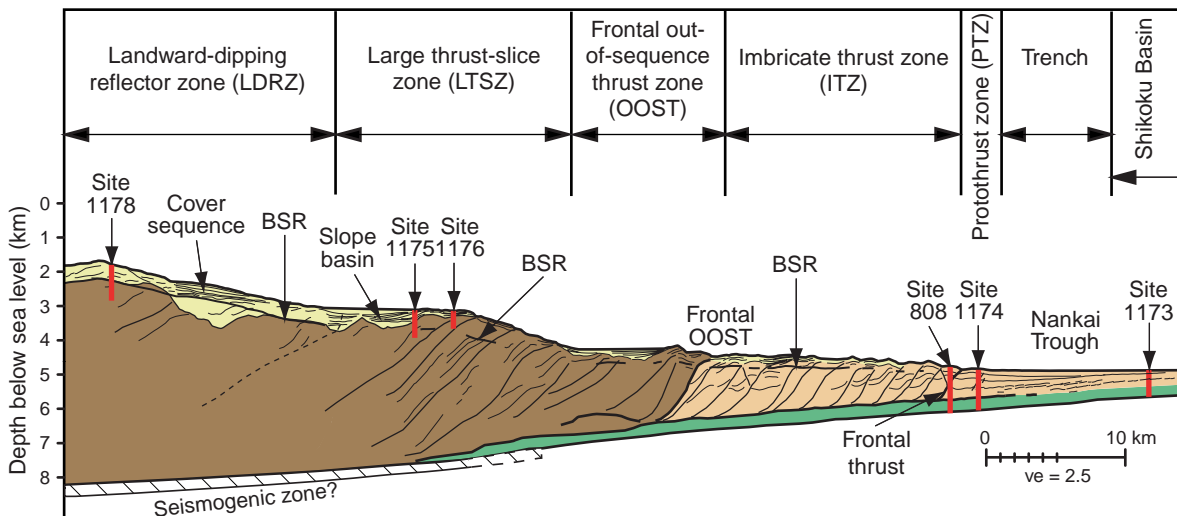
Figure F2. Dip angle of bedding, foliation, and fractures. Shaded areas show deformed intervals characterized by the development of fractures and brecciated zones. Note that there is an increase in fracturing at 550 mbsf but that it was not possible to measure the orientation of the structures.
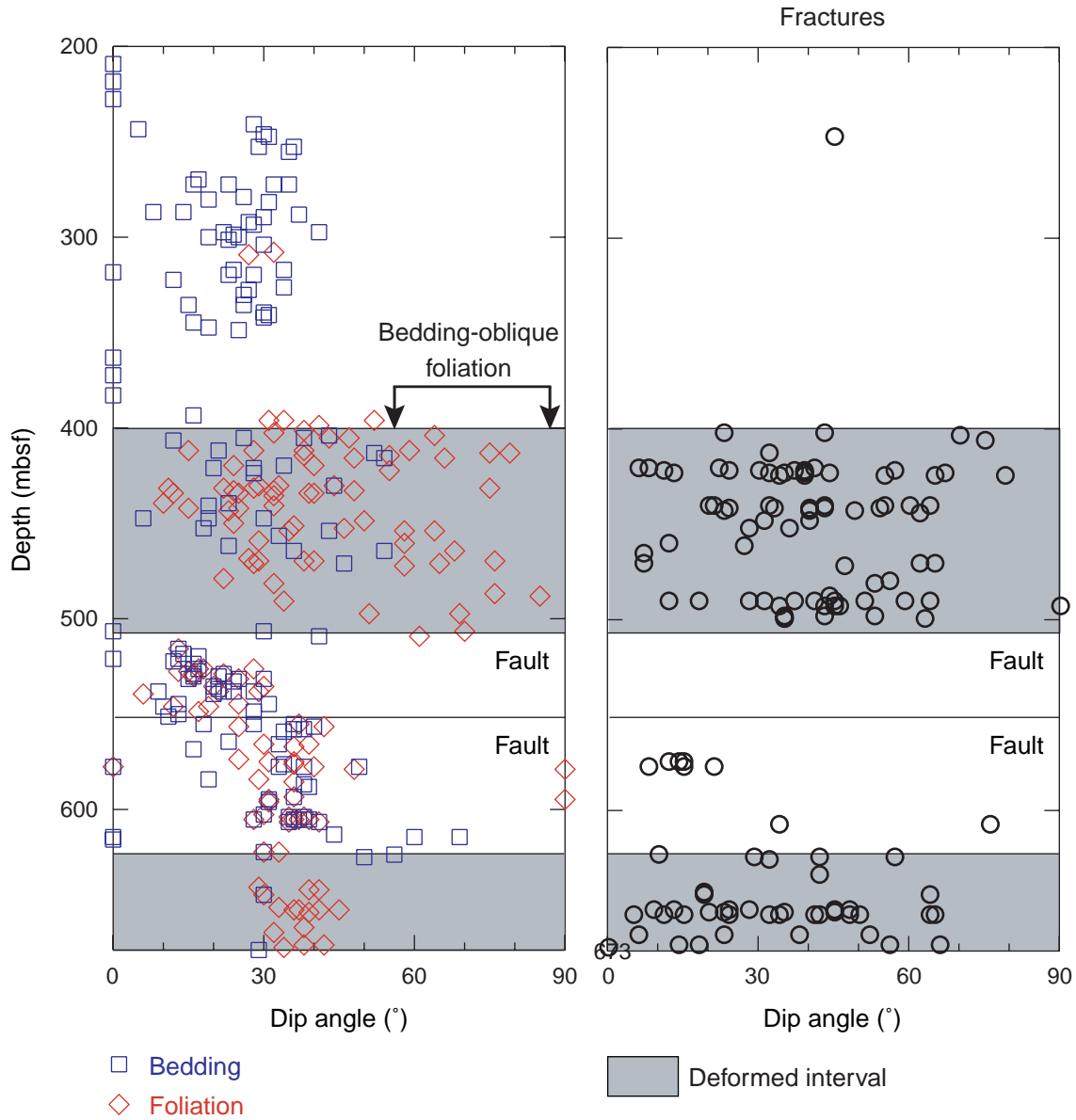
Figure F3. Deformation structures of accreted sediments at Site 1178. **A.** Core photograph of a brecciated zone in the deformed interval between 400 and 506 mbsf (Section 190-1178B-6R-2). **B.** Photomicrograph of black seams dipping in a single direction. Note the preferred orientation of phyllosilicates along seams (Sample 190-1178B-27R-2, 70–76 cm). **C.** Photomicrograph of black seams dipping in two directions. Note that sandy portions are cut and displaced by seams (Sample 190-1178B-27R-2, 70–76 cm). **D.** Photomicrograph of foliation in the deformed interval between 400 and 506 mbsf (Sample 190-1178B-8R-6, 53–57 cm). Phyllosilicates are parallel to sand lamina (dash lines) defining bedding-parallel fissility. **E.** Secondary mode SEM image of foliation in the deformed interval between 400 and 506 mbsf (Sample 190-1178B-4R-3, 50–52 cm). Although bedding cannot be discerned in this sample, the dip of foliation attains 79°, which is too steep for bedding-parallel foliation (see also Fig. F2, p. 12). **F.** Close-up photograph of bedding-oblique foliation (Section 190-1178B-8R-4).
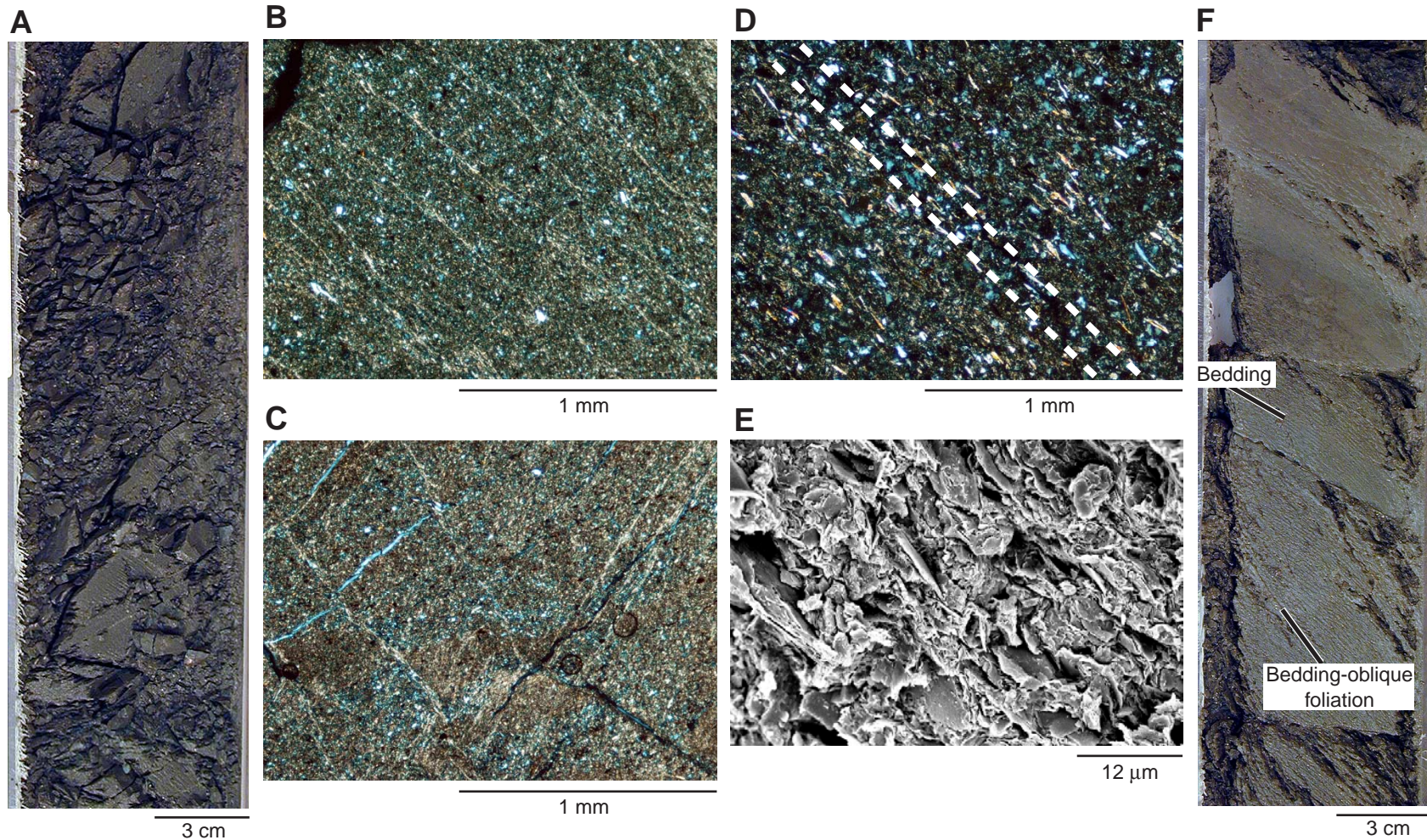
Figure F4. A. Magnetic susceptibility and dip angle of poles to magnetic foliation, bedding, and foliation vs. depth. Shaded areas indicate deformed intervals. Litho. unit = lithostratigraphic unit (Subunit IIA = accreted axial trench-wedge facies; Subunit IIB = accreted outer trench-wedge facies; and Subunit IIC = accreted axial trench-wedge facies). **B.** Distribution of principal susceptibility axes after paleomagnetic correction.
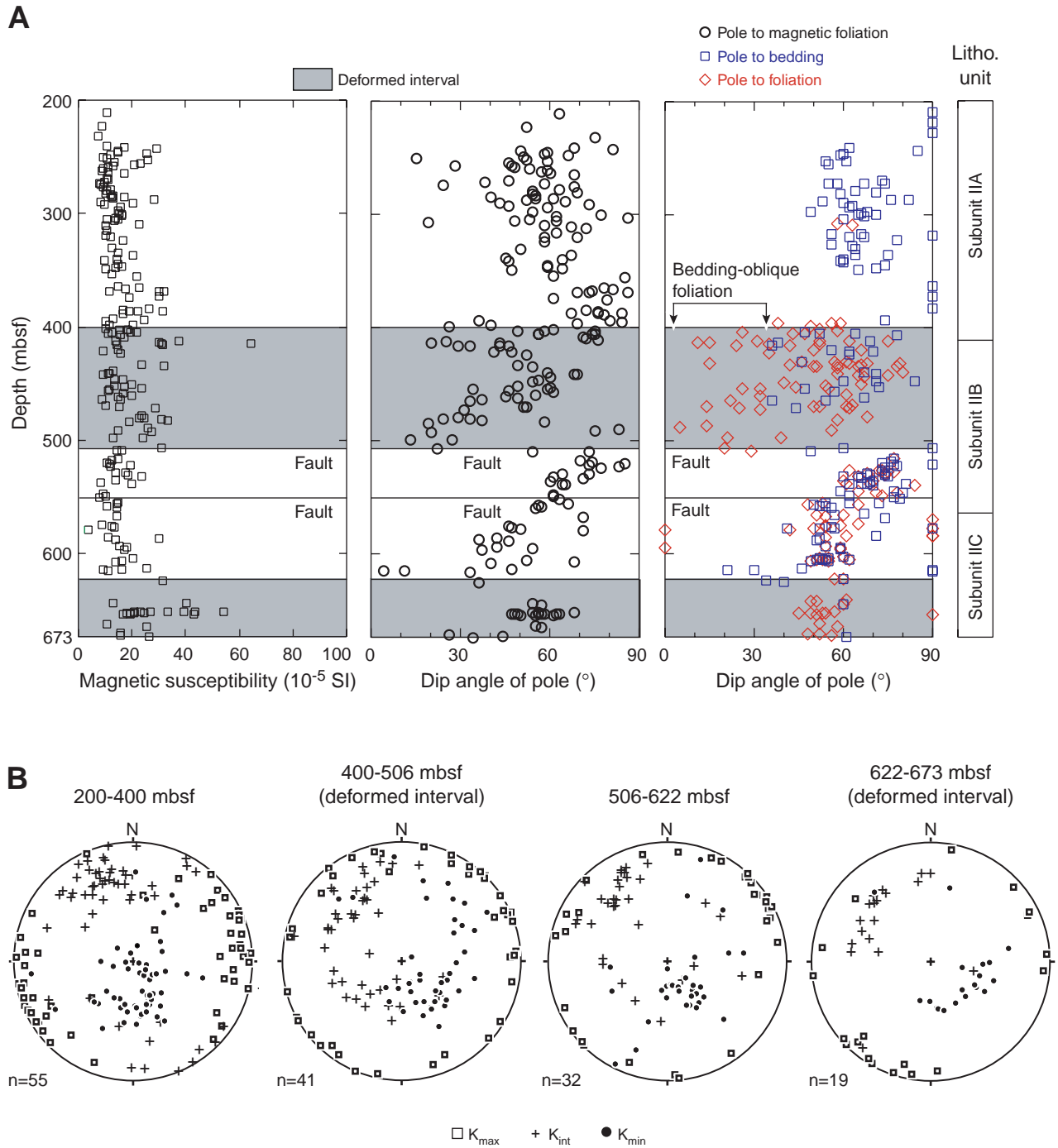
Figure F5. Summary of deformation structures and magnetic fabric in the Nankai accretionary prism at Site 1178.